Monthly Notices of the ROYAL ASTRONOMICAL SOCIETY

Mon. Not. R. Astron. Soc. **415,** 1534–1542 (2011) doi:10.1111/j.1365-2966.2011.18810.x

# Galactic fountains and the rotation of disc-galaxy coronae

Federico Marinacci,[1★] Filippo Fraternali,[1] Carlo Nipoti,[1] James Binney,[2] Luca Ciotti[1] and Pasquale Londrillo[3]

[1]*Astronomy Department, University of Bologna, via Ranzani 1, I-40127 Bologna, Italy*
[2]*Rudolf Peierls Centre for Theoretical Physics, Oxford University, Keble Road, Oxford OX1 3NP*
[3]*INAF-Bologna Astronomical Observatory, via Ranzani 1, I-40127 Bologna, Italy*

Accepted 2011 March 25. Received 2011 February 18

## ABSTRACT

In galaxies like the Milky Way, cold ($\sim 10^4$ K) gas ejected from the disc by stellar activity (the so-called galactic-fountain gas) is expected to interact with the virial-temperature ($\sim 10^6$ K) gas of the corona. The associated transfer of momentum between cold and hot gas has important consequences for the dynamics of both gas phases. We quantify the effects of such an interaction using hydrodynamical simulations of cold clouds travelling through a hot medium at different relative velocities. Our main finding is that there is a velocity threshold between clouds and corona, of about 75 km s$^{-1}$, below which the hot gas ceases to absorb momentum from the cold clouds. It follows that in a disc galaxy like the Milky Way a static corona would be rapidly accelerated; the corona is expected to rotate and to lag, in the inner regions, by $\sim$80–120 km s$^{-1}$ with respect to the cold disc. We also show how the existence of this velocity threshold can explain the observed kinematics of the cold extraplanar gas.

**Key words:** hydrodynamics – turbulence – ISM: kinematics and dynamics – Galaxy: kinematics and dynamics – Galaxy: structure – intergalactic medium.

## 1 INTRODUCTION

Current cosmological models suggest that galaxies are embedded in extended virial-temperature atmospheres called coronae. These coronae are thought to contain a significant fraction (more than 50 per cent) of the baryons in the Universe on the basis of a combination of big bang nucleosynthesis theory and observations of the cosmic microwave background (e.g. Fukugita, Hogan & Peebles 1998; Fukugita & Peebles 2004; Komatsu et al. 2009). In clusters of galaxies the baryons associated with the hot intracluster medium are directly detected in X-rays through their free–free emission (Sarazin 2009), whilst in lower density environments, such as the Local Group, the hot medium must be characterized by a much lower X-ray surface brightness, below the sensitivity of the current instrumentation (Anderson & Bregman 2010).

The existence of coronal gas around our Galaxy was hypothesized by Spitzer (1956) to provide the necessary pressure confinement to cold clouds of interstellar gas that lie far from the Galactic plane. With the advent of ultraviolet (UV) spectroscopy, highly ionized material (in particular C IV, O V and O VI) was detected along lines of sight to distant UV sources that pass close to high- and intermediate-velocity clouds (HVCs and IVCs, see Sembach et al. 2003; Fox, Savage & Wakker 2006). These clouds are not massive enough to be confined by self-gravity and the detected species are believed to lie at the interface between the coronal gas with $T \gtrsim 10^6$ K, and the HVCs/IVCs, which are composed by cooler and partly neutral gas.

In star-forming disc galaxies, high-sensitivity H I observations have revealed that roughly 10 per cent of the neutral gas is outside the thin disc, at distances of a few kiloparsecs (Oosterloo, Fraternali & Sancisi 2007; Fraternali 2009, and references therein). The origin of this extraplanar gas is not completely understood but it is now widely accepted that a large fraction of it is produced by supernova-powered bubbles which drive neutral and partly ionized gas out of the galactic disc. This gas is expected to travel through the halo and eventually to fall back to the disc in a time-scale of $\sim$80–100 Myr, a mechanism which is known as galactic fountain (Shapiro & Field 1976; Bregman 1980; Houck & Bregman 1990). Thus, in the regions within a few kiloparsecs from the galactic disc a large number of galactic-fountain 'cold' clouds (IVCs in the Milky Way) should be travelling through the ubiquitous coronal gas and an interaction between the two phases is inevitable, with important consequences for the kinematics of both.

Unfortunately, the kinematics of the coronal gas is virtually unconstrained; as mentioned, most of the evidence for this gas is indirect, and from the available data it is not possible to extract reliable kinematic information. A potentially useful direct detection comes from the observation of O VII absorption lines (which probe material at temperatures around $10^6$ K) towards bright quasars (e.g. Rasmussen et al. 2003). However due to the poor spectral resolution of the current X-ray instruments, these observations are impractical (Bregman & Lloyd-Davies 2007; Yao et al. 2008).

★E-mail: federico.marinacci2@unibo.it

On the other hand, the kinematics of the extraplanar cold gas has been studied extensively with H I and optical line data (Swaters, Sancisi & van der Hulst 1997; Fraternali et al. 2005; Heald et al. 2007; Oosterloo et al. 2007; Kamphuis 2008). It was found that the extraplanar gas rotates with a speed that decreases steadily with increasing distance from the mid-plane of the galaxy. A number of models have been proposed to explain this vertical velocity gradient (e.g. Barnabè et al. 2006; Kaufmann et al. 2006; Melioli et al. 2009; Struck & Smith 2009; Marinacci et al. 2010b). In particular, it has been shown that the *rotational* gradient is larger than what would be expected for a collection of galactic-fountain clouds that travel through the halo region on pure ballistic trajectories (Fraternali & Binney 2006), so the natural next step is to consider how clouds' trajectories are affected by interactions with the ambient corona.

Fraternali & Binney (2008, hereafter FB08) considered two types of cloud–corona interaction: drag and accretion. The drag between the H I clouds and a supposedly lagging corona was proposed, among others by Collins, Benjamin & Rand (2002) and Barnabè et al. (2006), to explain the negative vertical rotation gradient of the extraplanar gas. However, FB08 showed that this mechanism is not viable because of the resulting rapid acceleration of the corona, which causes the drag to vanish in less than a cloud orbital time. Thus, if the drag is as efficient as one would expect from purely mechanical arguments, the corona should rotate at a speed comparable to that of the disc, with a consequent vanishing of the drag. FB08 then investigated the possibility that H I clouds accrete some of the ambient gas that lies in their paths. They showed that if the ambient gas has a relatively low angular momentum about the galaxy's spin axis, its accretion on to H I clouds could explain the observed dynamics of the fountain clouds.

In a preliminary study, Marinacci et al. (2010a, hereafter M10) presented hydrodynamical simulations of cold clouds travelling through a hot medium with properties similar to the gas of a galactic corona. They found that radiative cooling can be efficient in the turbulent wakes of the clouds, allowing coronal material to condense in these wakes. Therefore, even though the original cloud is ablated, there is a net transfer of mass from the corona to the whole body of cool gas, supporting the FB08 framework.

In this paper we extend the study of the interaction between the clouds and the corona presented by M10 in two ways: (i) we use an upgraded version of the hydro-code taking into account the variation in the mean molecular weight of the gas at $T \simeq 10^4$ K (mainly due to hydrogen recombination) and, more importantly, the different metallicity of the disc and of the coronal gas; (ii) we study a much wider range of relative cloud–corona velocities. Our major finding is that there is a velocity threshold between cloud and corona below which the corona does not absorb momentum from the cloud. We argue that the corona must be spinning fast enough for most clouds to move through the corona at a speed smaller than this velocity threshold. This prediction will be tested by future soft X-ray observations.

The paper is organized as follows. Section 2 explains which simulations were run, and the results of these simulations are analysed in Section 3; in Section 4 we discuss the implications of our results for the kinematics of both the corona and the clouds, while Section 5 sums up.

## 2 SET-UP OF THE HYDRODYNAMICAL SIMULATIONS

The initial conditions of the simulations are similar to those of M10; we simulate a cloud at $T = 10^4$ K with radius $R_{\rm cl} = 100$ pc that moves at a speed $v_0$ through a stationary and homogeneous background at $T = 2 \times 10^6$ K, which represents the corona. While in M10 the *relative* speed between the cloud and the corona was fixed at $v_0 = 75\,{\rm km\,s^{-1}}$, here we explore different relative speeds in the range $50 \leq v_0 \leq 200\,{\rm km\,s^{-1}}$. If these relative speeds are interpreted as differences in rotational velocities, then two extreme possibilities are encompassed by the simulations: (i) the case of a non-rotating corona ($v_0 = 200\,{\rm km\,s^{-1}}$) and (ii) a corona which is rotating with a speed close to that of the disc ($v_0 = 50\,{\rm km\,s^{-1}}$). As on ballistic trajectories the galactocentric radii of the clouds would vary by less than 30 per cent, and the clouds would reach heights above the galactic plane of a few kiloparsecs (see Fraternali & Binney 2006), the expected density variations of the coronal gas are not strong. Thus, as in M10, we simplify our treatment by assuming a homogeneous corona and neglecting the effect of the gravitational field of the galaxy. We also neglect the self-gravity of the gas, because the cloud masses are much smaller than their Jeans mass. At the beginning of each simulation the cloud is in pressure equilibrium with its surroundings and the evolution of the system is followed for 60 Myr (significantly longer than the 25 Myr spanned by most runs in M10). In our standard simulations (see Table 1) the density of the background is $n = 10^{-3}\,{\rm cm^{-3}}$. For each value of $v_0$, we ran two simulations: one (dissipative) in which the gas is allowed to cool radiatively, another (adiabatic) without radiative cooling. The more realistic cases are those in which the gas is allowed to cool, but the adiabatic runs enable us to distinguish the effect of cooling (strongly dependent on the density, temperature and metallicity of the gas) from non-dissipative effects like mixing and hydrodynamical instabilities. Two additional sets of dissipative simulations have been run with half (low-density simulations in Table 1) or twice (high-density simulations in Table 1) the coronal density to assess the influence of this latter on the results. In all initial conditions the cloud's metallicity $Z_{\rm cl}$ takes the solar value $Z_\odot$ and the coronal metallicity is $Z_{\rm cor} = 0.1\,Z_\odot$ (see e.g. Sembach et al. 2003; Shull et al. 2009). The metallicity of the fluid is allowed to vary from the initial conditions: in this respect the present simulations differ from those of M10, in which the metallicity was constant. This upgrade is

**Table 1.** Parameters of the simulations. The initial temperature and metallicity of the corona are $T_{\rm cor} = 2 \times 10^6$ K and $Z_{\rm cor} = 0.1\,Z_\odot$, respectively, while for the cloud $T_{\rm cl} = 10^4$ K and $Z_{\rm cl} = Z_\odot$. All models are evolved up to 60 Myr. The grid size is 6114×1024 with spatial resolution ∼2 × 2 pc for all the simulations. In the case of v100 an additional run, with the same spatial resolution and grid size 6144×2048, was performed.

| Simulation | $v_0$ ($\rm km\,s^{-1}$) | $n_{\rm cor}$ ($\rm cm^{-3}$) | $M_{\rm cl}$ ($10^4\,M_\odot$) |
|---|---|---|---|
| | Standard simulations | | |
| v200 | 200 | $10^{-3}$ | 2.4 |
| v150 | 150 | $10^{-3}$ | 2.4 |
| v100 | 100 | $10^{-3}$ | 2.4 |
| v75 | 75 | $10^{-3}$ | 2.4 |
| | High-density simulations | | |
| v100–h | 100 | $2 \times 10^{-3}$ | 4.8 |
| v75–h | 75 | $2 \times 10^{-3}$ | 4.8 |
| | Low-density simulations | | |
| v100–l | 100 | $5 \times 10^{-4}$ | 1.2 |
| v75–l | 75 | $5 \times 10^{-4}$ | 1.2 |
| v50–l | 50 | $5 \times 10^{-4}$ | 1.2 |

important since the metallicity of a cloud ejected from the disc and that of the corona can differ by one order of magnitude or more, and the cooling rate of the gas critically depends on its metal content. In any case, we stress that the main results of M10 are confirmed by the present investigation: for instance, the global behaviour of M10 simulation with $n = 10^{-3}\,\mathrm{cm}^{-3}$ and *uniform* metallicity $Z = 0.3\,\mathrm{Z}_{\odot}$ is similar to ours with the same initial coronal density and cloud speed, but $\mathrm{Z}_{\mathrm{cl}} = \mathrm{Z}_{\odot}$ and $\mathrm{Z}_{\mathrm{cor}} = 0.1\,\mathrm{Z}_{\odot}$.

The simulations are performed with ECHO, a high-order, shock-capturing Eulerian hydrodynamical code: a detailed description and tests of it can be found in Del Zanna & Bucciantini (2002) and Del Zanna et al. (2007). In the current version of the code (ECHO++) not only the metallicity evolves, but also the fluid's molecular weight $\mu$ is a function of temperature. The variation of $Z$ and $\mu$ is accounted for in the implementation of radiative cooling, which is modelled according to the prescription of Sutherland & Dopita (1993). The calculations are performed on a two-dimensional Cartesian grid with open boundary conditions imposed to all the sides of the computational domain. Therefore, one of the dimensions perpendicular to the cloud's velocity has been suppressed, and we are in effect simulating a flow around an infinite cylindrical cloud. The cylinder is moving perpendicular to its long axis and has initially a circular cross-section of radius $R_{\mathrm{cl}}$. From the simulations we obtain quantities per unit length of the cylinder and we relate these to the corresponding quantities for an initially spherical cloud of radius $R_{\mathrm{cl}}$ by multiplying the cylindrical results by the length $(4/3)R_{\mathrm{cl}}$ within which the mass of the cylinder equals the mass of the spherical cloud. This correction is included in the values of the cloud mass $M_{\mathrm{cl}}$ quoted in Table 1. We note that, due to pressure equilibrium in the initial conditions, for the same gas number density, temperature and cloud size $M_{\mathrm{cl}}$ is higher here than in M10, because here we account for the fact that $\mu$ depends on temperature, while in M10 $\mu$ is fixed at the coronal value.

## 3 RESULTS OF THE SIMULATIONS

We now describe the results of the hydrodynamical simulations, with emphasis on the mass and momentum transfer between the cloud and the ambient gas. While the two phases are unambiguously separated in the initial conditions (the cloud gas is at $T = 10^4\,\mathrm{K}$ and the coronal gas is at $T = 2 \times 10^6\,\mathrm{K}$), at later times, as a consequence of turbulent mixing and radiative cooling, we expect to have a significant amount of gas at intermediate temperatures. Therefore, at all times in the simulations, we define 'hot' the gas at $T > 10^6\,\mathrm{K}$ and 'cold' the gas at $T < 3 \times 10^4\,\mathrm{K}$, identifying the hot phase with the corona and the cold phase with the cloud. We verified that our results do not depend significantly on the specific choice of these temperature cuts.

### 3.1 Interaction between the cloud and the ambient medium

Qualitatively, the evolution of the cloud in the present simulations is similar to that observed in the simulations of M10. Due to the ram pressure arising from the motion, the cloud feels a drag which causes it to decelerate while the background gains momentum. The body of the cloud is squashed, and behind it a wide turbulent wake forms, in which the coronal and cloud gas mix efficiently and radiative cooling is particularly effective, with the consequence that the cloud mass tend to increase with time. The wake has a complex velocity structure, with some fluid elements moving faster and other slower than the body of the cloud.

This behaviour is apparent from Figs 1 and 2, showing, respectively, density and velocity snapshots, at four different times, of the dissipative standard simulation with $v_0 = 100\,\mathrm{km\,s}^{-1}$ (right-hand panels) and, for comparison, of the corresponding adiabatic simulation (left-hand panels). The diagrams in the bottom panels clearly show that the cloud is decelerated by drag: at

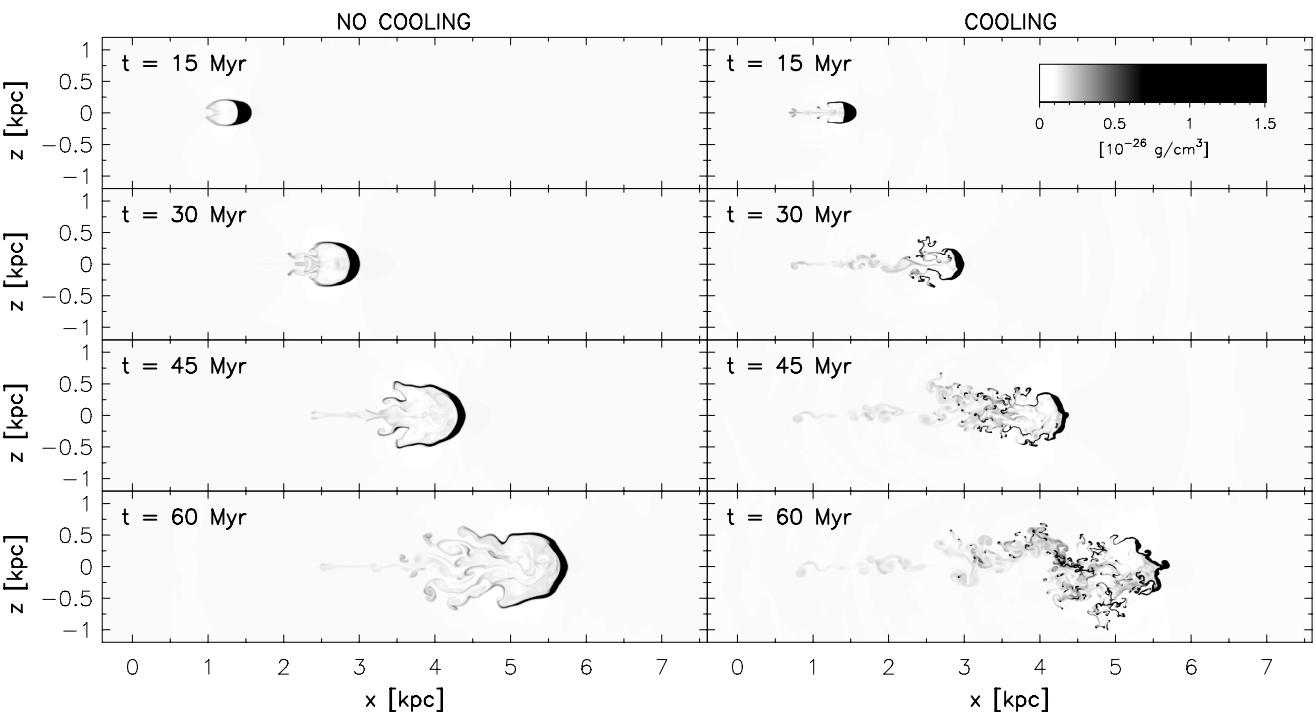


**Figure 1.** Density snapshots of the adiabatic (left-hand panels) and dissipative (right-hand panels) standard simulations with $v_0 = 100\,\mathrm{km\,s}^{-1}$ (v100 in Table 1). The time at which the snapshot has been taken is indicated in each panel. The initial position of the cloud centre is $x = 0$.

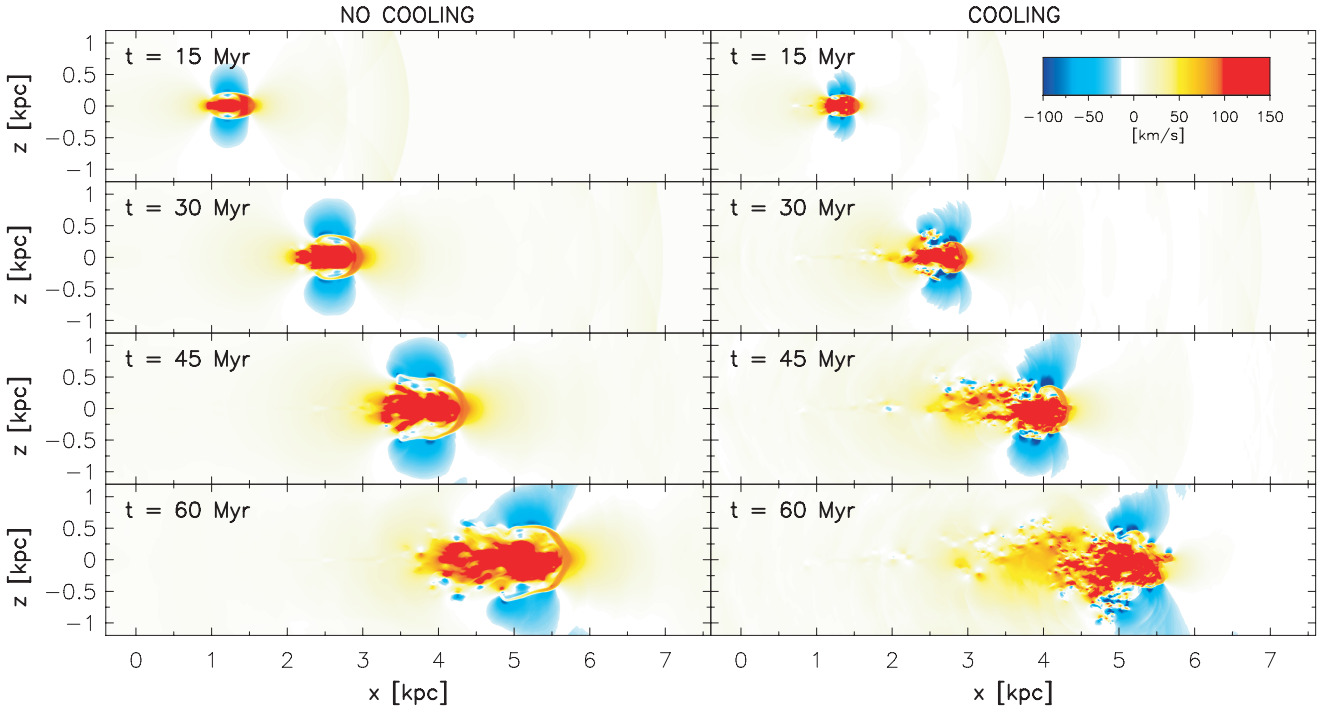


**Figure 2.** Same as Fig. 1, but plotting the velocity along the cloud's direction of motion ($v_x$).

$100\,\mathrm{km\,s^{-1}} \simeq 0.1\,\mathrm{kpc\,Myr^{-1}}$ the cloud would travel, with no drag, a distance of about 6 kpc in 60 Myr, but neither in the presence nor in the absence of radiative cooling does the main body of the cloud reach that distance. The structure of the body of the cloud and of the wake is strongly influenced by the presence of radiative cooling; the wake is more elongated and less laterally extended (except perhaps in the 60 Myr panel) when the radiative cooling of the gas is permitted. The extent of the velocity structure of the wake is greater, both laterally and in elongation, in the dissipative than in the adiabatic case at late times (see Fig. 2). Just behind the cloud there is a region in which the velocities reach their maximum values and this region is more compact (less elongated) when cooling occurs. In front of the cloud the coronal gas is pushed by the cloud and therefore also in this region the gas has positive velocity. However, in contrast to what happens behind the main body of the cloud, this region is more extended in the absence of cooling.

Comparing the final configuration with the initial conditions, we find that the cloud has increased its mass (when cooling is allowed) and that the corona has gained momentum. Quantitatively, the amount of mass and momentum transfer depends critically on radiative cooling. This can be seen in Fig. 3, which shows the distributions of mass (upper panel) and momentum (lower panel) as functions of temperature after 50 Myr for the standard simulation with $v_0 = 100\,\mathrm{km\,s^{-1}}$ and, for comparison, for its adiabatic counterpart. In both panels the histograms peak around the temperatures of the coronal gas and the initial cloud temperature ($T = 2 \times 10^6$ and $10^4$ K, respectively), and the distribution around these peaks is rather narrow. From the bottom panel of Fig. 3 it is clear that there is an exchange of momentum between the cloud and the corona, but the corona acquires *less* momentum when the gas is allowed to cool, as can be inferred from the heights of the peaks at $T > 10^6$ K. This can be better understood if we recall how the mass of the gas is distributed among the various phases. At the beginning, most of the gas is at the cloud and the corona initial temperatures, and only a small fraction of the total mass is at intermediate temperatures. The momentum of the cloud is mostly transferred to this intermediate temperature component as a result of the mixing. Because this gas is in the temperature range $T \simeq 1$–$5 \times 10^5$ K, in which the cooling function reaches its maximum, it can cool very effectively. The consequence of this cooling is a mass transfer from the corona towards the cold gas. The momentum removed from the cold cloud is thus retained by the cooling gas and never transferred to the coronal gas. If the cooling is not present, the process of condensation of the mixed gas cannot occur and therefore the cloud continues to transfer its momentum to the mixed gas and thus to the corona.

### 3.2 Motion of the cold gas

In order to quantify the deceleration of the cold cloud, in the simulations we monitor the evolution of its centroid velocity, defined as the total momentum of the cold gas in the cloud's direction of motion $x$ divided the total mass of the cold gas. We compare the centroid velocity with the analytic estimate (FB08)

$$v(t) = \frac{v_0}{1 + t/t_{\mathrm{drag}}}, \tag{1}$$

where the characteristic drag time is given in terms of the cloud's initial mass $M_{\mathrm{cl}}$, geometrical cross-section $\sigma$, and coronal density $\rho_{\mathrm{h}}$, by

$$t_{\mathrm{drag}} = \frac{M_{\mathrm{cl}}}{v_0 \sigma \rho_{\mathrm{h}}}. \tag{2}$$

In all our dissipative standard simulations, independent of the initial speed $v_0$, after 60 Myr the centroid velocity is $\sim 0.75\,v_0$, significantly lower than the values predicted by equation (1), which treats the cloud as a rigid body. This discrepancy is due to a combination of cloud deformation, hydrodynamical instabilities and condensation of cooling gas. This can be inferred from Fig. 4, which shows the centroid velocity for the dissipative (stars) and adiabatic (plus signs) standard simulations with $v_0 = 200\,\mathrm{km\,s^{-1}}$ (top), $v_0 = 100\,\mathrm{km\,s^{-1}}$

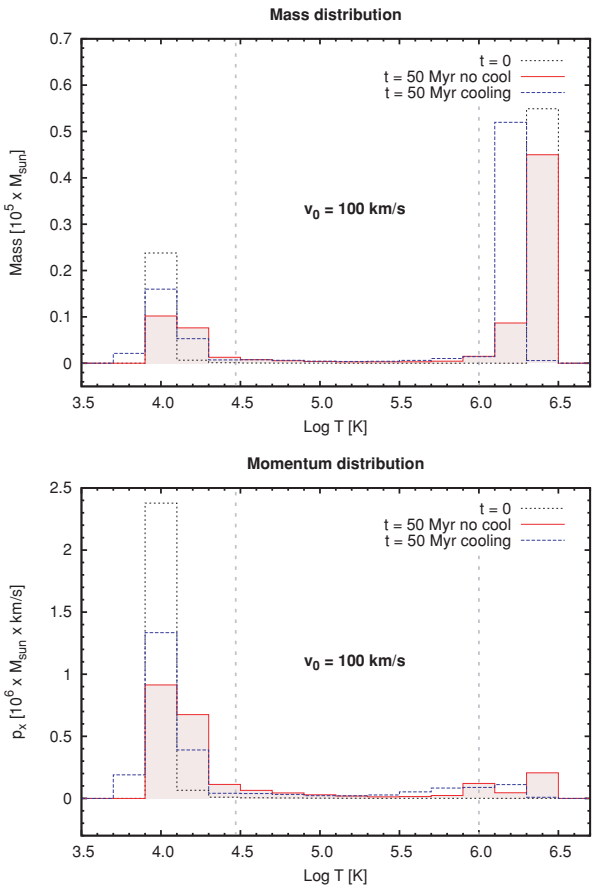


**Figure 3.** Distributions of mass (upper panel) and momentum (lower panel) as functions of the gas temperature after 50 Myr of evolution of the the adiabatic (shaded) and dissipative (long-dashed line) standard simulations with $v_0 = 100\,\mathrm{km\,s^{-1}}$; the black short-dashed line is the initial mass or momentum distribution. The vertical grey dashed lines represent the temperature cuts used to define cold and hot gas phases.

(centre) and $v_0 = 75\,\mathrm{km\,s^{-1}}$ (bottom). It is clear that the analytic formula (solid line in each diagram) is a good description of the general behaviour of cold gas motion over ∼60 Myr only when the cooling is not allowed and the initial relative speed is sufficiently low (see bottom panel in the figure). When these conditions are not satisfied, the analytic formula fails after some time, mainly because Kelvin–Helmholtz instability strips some cold gas and the ram pressure progressively squashes the cloud increasing its cross-section. The net effect is an enhancement of drag effectiveness (see equation 2).

Let us now compare the evolution of the centroid velocity in the presence and in the absence of cooling. First, it must be noticed that in normalized units ($v_0$ for velocities and $R_{\rm cl}/v_0$ for times, shown in the right and upper axes in the diagrams in Fig. 4) the evolution of the centroid velocity is basically the same in all the adiabatic simulations (in the overlapping normalized time intervals). In particular, the deviation from the analytic estimate becomes apparent at roughly the same normalized time and it can be ascribed mainly to the flattening of the main body of the cloud. In the presence of cooling, the deviation of the cloud speed from the analytic estimate is remarkably insensitive to the initial speed, but if anything it decreases as the initial speed increases, at least at the highest speeds. In these dissipative cases the amount of gas that transfers from the hot to the cold phase has an appreciable impact on the centroid

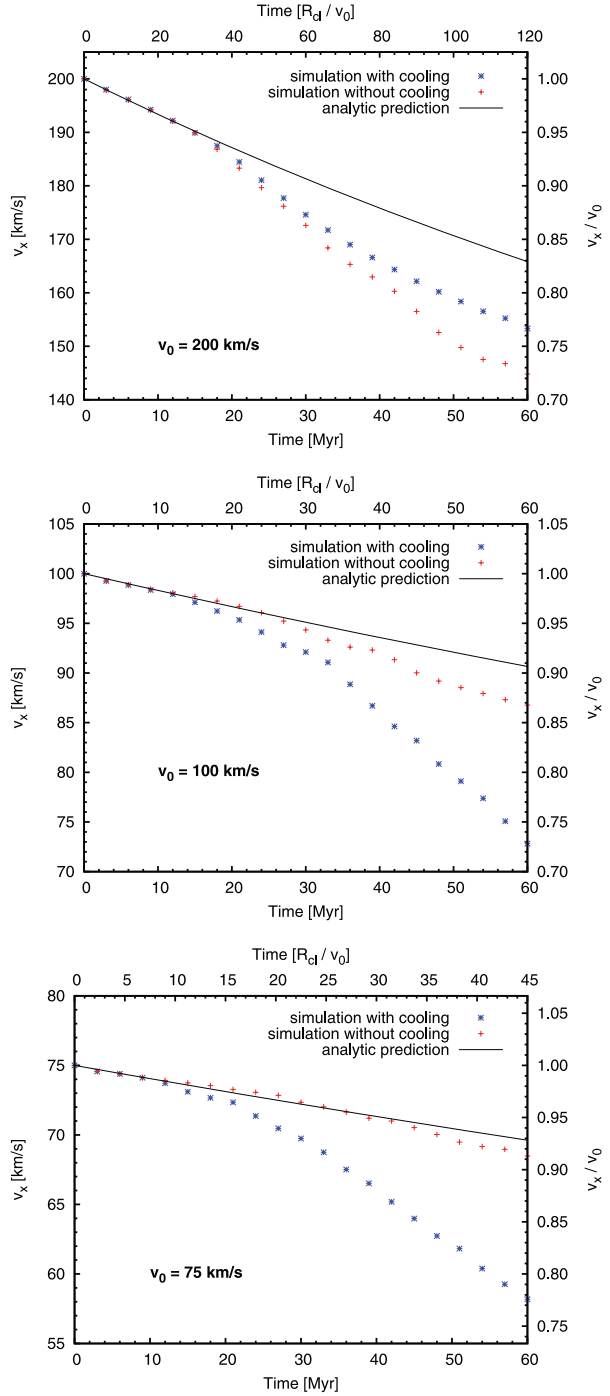


**Figure 4.** Evolution of the centroid velocity, along the cloud's direction of motion, of cold gas in the dissipative (stars) and adiabatic (plus signs) standard simulations with $v_0 = 200\,\mathrm{km\,s^{-1}}$ (top panel), $v_0 = 100\,\mathrm{km\,s^{-1}}$ (central panel) and $v_0 = 75\,\mathrm{km\,s^{-1}}$ (bottom panel). The solid lines are the theoretical predictions in the case of a quadratic drag (equation 1).

velocity, so we are no longer merely looking at the slowing of the original cloud, and the deceleration is dominated by condensation of cooling material that was originally at rest.

### 3.3 Momentum of the hot gas

We now turn to the momentum transferred to the hot gas. In the simulations, the total momentum of the hot gas is computed by

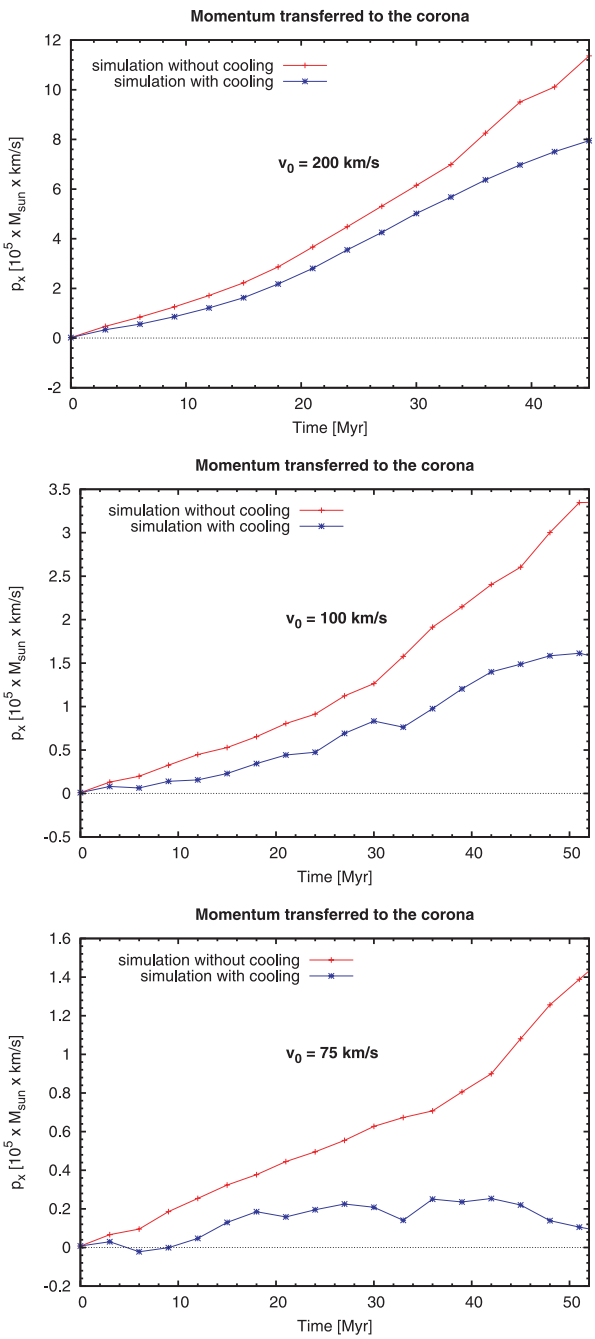


**Figure 5.** Evolution of momentum acquired by the corona as a function of time in the dissipative (stars) and adiabatic (plus signs) standard simulations with $v_0 = 200, 100, 75\,\mathrm{km\,s^{-1}}$ (from top to bottom). For comparison, we note that the total initial momentum of the cloud is $2.4 \times 10^6\,(v_0/100\,\mathrm{km\,s^{-1}})$.

summing, over the whole computational domain, the momentum of the cells containing gas at $T > 10^6$ K. Fig. 5 shows the amount of momentum, along the cloud's direction of motion $x$, acquired by the hot gas as a function of time for the dissipative (stars) and adiabatic (plus signs) standard simulations with $v_0 = 200, 100, 75\,\mathrm{km\,s^{-1}}$. From these diagrams it is apparent that the hot gas gains less momentum in the presence than in the absence of radiative cooling. The ratio between the final coronal momentum in the dissipative and in the adiabatic simulations is ~0.8 when $v_0 = 200\,\mathrm{km\,s^{-1}}$ (top panel), ~0.5 when $v_0 = 100\,\mathrm{km\,s^{-1}}$ (middle panel), and $\lesssim$0.1 when $v_0 = 75\,\mathrm{km\,s^{-1}}$ (bottom panel). In particular, when $v_0 = 75\,\mathrm{km\,s^{-1}}$ the momentum transferred from the cold gas to the corona, after an initial phase of growth lasting for ~20 Myr, settles to a nearly constant value: from that moment onwards, the momentum transferred to the corona is consistent with zero. Thus, the simulations indicate the existence of a *velocity threshold* $v_{\rm th}$ below which the transfer of momentum from the cold clouds to the corona is suppressed. Given that the cloud keeps losing momentum (Fig. 4) and the total momentum is conserved, it follows that the momentum lost by the cloud is retained by the coronal gas, which is progressively cooling on to the cloud's wake.

The measure of the momentum transferred from the cold to the hot gas can be affected by the flow of coronal gas (and associated momentum) through the open boundaries of the computational domain. This effect becomes non-negligible only in the last ~10 Myr of the simulations, so we take ~50 Myr as final time, as far as the measure of the coronal momentum is concerned (see also Fig. 3). As an additional test, we also ran a simulation with the same initial condition as the standard simulation with $v_0 = 100\,\mathrm{km\,s^{-1}}$, but with twice the number of grid points in the direction perpendicular to the cloud's direction of motion (keeping the resolution fixed and thus effectively doubling the size of the domain), finding relative differences in the actual value of the coronal momentum within 8 per cent.

Since the density of the corona strongly influences the cooling rate of the gas, we tested whether the velocity threshold depends on this parameter with two additional sets of simulations with half and twice the above coronal density. In particular we ran two simulations with higher density ($v_0 = 75, 100\,\mathrm{km\,s^{-1}}$) and three simulations with lower density ($v_0 = 50, 75, 100\,\mathrm{km\,s^{-1}}$; see Table 1). In a denser corona, due to the increased cooling rate, the value of the velocity threshold rises to $\approx$85 km s$^{-1}$. In the case of the less dense corona, we found that momentum is transferred significantly also when $v_0 = 75\,\mathrm{km\,s^{-1}}$, but when $v_0 = 50\,\mathrm{km\,s^{-1}}$ the momentum transfer is consistent with zero, so $v_{\rm th} \approx 50\,\mathrm{km\,s^{-1}}$. This means that the actual value of the velocity threshold $v_{\rm th}$ is sensitive to the coronal density, and therefore uncertain. However, provided that in Milky Way like galaxies the actual average coronal density a few kiloparsecs above the plane is in the explored interval 0.5–2 × $10^{-3}\,\mathrm{cm^{-3}}$, we can consider $v_{\rm th} \sim$ 50–85 km s$^{-1}$ as a fiducial range for the velocity threshold.

## 4 IMPLICATIONS FOR GALACTIC CORONAE AND COLD EXTRAPLANAR GAS

### 4.1 Rotating coronae

FB08 showed that if a significant part of the momentum lost by H I clouds through ram-pressure drag is absorbed by the corona, the spin of the latter will increase on a time-scale that is short even compared to the orbital time (~100 Myr) of an individual cloud. If the corona did not rotate, the velocity differences between it and individual clouds would be dominated by the cloud's azimuthal motion, and being $\gtrsim$200 km s$^{-1}$ would exceed the velocity threshold $v_{\rm th}$. Consequently, the corona would gain a significant fraction of the momentum lost by clouds, acquiring substantial angular momentum on a short time-scale. Hence the rotation rate of the corona must be determined by the condition that the relative velocity of a typical cloud and the corona is $\lesssim v_{\rm th}$. Since clouds are travelling with an average vertical velocity $\langle v_z \rangle \sim 40\,\mathrm{km\,s^{-1}}$ (Marasco & Fraternali 2011), the rotational lag required for this condition to be satisfied is $v_{\rm lag} \sim \sqrt{v_{\rm th}^2 - \langle v_z \rangle^2}$. For the estimate of $v_{\rm th} \approx 75\,\mathrm{km\,s^{-1}}$ given

above, we obtain $v_{\rm lag} \sim 65\,{\rm km\,s^{-1}}$. Thus, we expect coronae to be quite rapidly rotating.

To compute the difference in rotation velocity between the corona and the disc at a given height, one must subtract the value for $v_{\rm lag}$ determined above to the value of the rotation velocity of the H I at that height. In the Milky Way, assuming a vertical gradient for the H I of $\simeq -15\,{\rm km\,s^{-1}\,kpc^{-1}}$ (Marasco & Fraternali 2011), we find that this difference is $\sim$95 km s$^{-1}$ at $z \simeq 2$ kpc, corresponding to a coronal rotation velocity of $\sim$125 km s$^{-1}$ for $v_\odot = 220\,{\rm km\,s^{-1}}$.

The fact that the corona is rotating, even at speeds lower than that of the galactic disc, has important consequences for its morphology. In general, the azimuthal velocity $v_\varphi$ of the corona can depend on both distance from the centre $R$ and height above the plane $z$, as is the case of baroclinic distributions (Poincaré–Wavre theorem; Lebovitz 1967; Tassoul 1978; Barnabè et al. 2006). The $z$ dependence might be expected in analogy with the observed kinematics of the cold extraplanar gas, and also as a consequence of the momentum transfer between fountain clouds and hot gas. By recalling the procedure outlined above, the lag of the corona with respect to the disc should vary from $\sim$70 to 120 km s$^{-1}$ going from $z = 0.5$ to 4 kpc, which is the typical region where fountain clouds are located. This corresponds to a rotational velocity of $\approx$150–100 km s$^{-1}$, assuming again $v_\odot = 220\,{\rm km\,s^{-1}}$. However, given the large uncertainty on the properties of the corona, here we consider much simpler (barotropic) models of coronae, in which $v_\varphi = v_\varphi(R)$. In particular, we construct isothermal ($T = 2 \times 10^6$ K) models of coronae in equilibrium in the axisymmetric gravitational potential of the Milky Way, as given by Binney & Tremaine (2008), with rotation law

$$v_\varphi(R) = v_{\rm s}\frac{R}{R + R_{\rm s}}. \tag{3}$$

The rotation is null at the centre and raises up to the terminal value $v_{\rm s}$; the rise of the rotation velocity is steeper for smaller values of $R_{\rm s}$. To match the expected rotational velocity range, in Fig. 6 the isodensity contours of two models with $v_{\rm s} = 100\,{\rm km\,s^{-1}}$ (upper panel) and $v_{\rm s} = 150\,{\rm km\,s^{-1}}$ (lower panel) are presented. In both cases $R_{\rm s} =$ 1 kpc. The resulting gas distributions are peanut-shaped, with axis ratio of the isodensity surfaces in the range 0.5–0.7. Therefore, if galactic coronae rotate with speeds of the order of those predicted by our model, they will appear significantly flattened when detected in future X-ray observations. We note that this peanut–shaped structure is also predicted in the general baroclinic case (Barnabè et al. 2006).

The kinematic properties of the galactic coronae are important also for their evolution. For instance, the thermal-stability properties of a corona can be significantly influenced by the distribution of specific angular momentum (Nipoti 2010), with implications for the origin of the HVCs (Binney, Nipoti & Fraternali 2009). However, the HVCs are typically thought to be relatively far from the disc, in a region not strongly affected by disc activities, while in the present work we have focused on the kinematics of the corona within a few kiloparsecs from the disc, where the galactic fountain is at work. It is not clear to what degree the kinematics of the hot gas far from the disc (which is likely related to the formation history of the galaxy) can be influenced by the kinematics of coronal gas near the disc.

### 4.2 Vertical velocity gradient of the cold extraplanar gas

The simulations presented here clearly indicate that clouds of cold gas ejected above the disc plane can lose angular momentum via interaction with the hot medium. This mechanism appears as a natural explanation for the observed vertical gradient in the rotation velocity of the extraplanar gas of disc galaxies. Unfortunately, a comparison between the results of the simulations and the observations is not straightforward, mainly because of the idealized nature of the simulations, in which we do not include the galaxy's gravitational field and thus we do not follow the cloud's orbit above the plane. However, our results can be used to obtain a rough estimate of the expected vertical rotational gradient of the extraplanar gas, using the following argument. Let us simplify the treatment by assuming that a cloud, ejected with a velocity orthogonal to the disc plane at some radius $R$, falls back on to the plane, after a time of the order of 100 Myr, at about the same radius $R$. Assuming a mean velocity for the ascending part of the orbit $\langle v_z \rangle = 40\,{\rm km\,s^{-1}}$ (Marasco & Fraternali 2011) and a mean maximum height above the disc for the cold clouds $\langle z_{\rm max} \rangle = 2$ kpc, the time to reach the maximum height is

$$t_{\rm orb} = \frac{\langle z_{\rm max} \rangle}{\langle v_z \rangle} \approx 50\,{\rm Myr}\,. \tag{4}$$

Thus, neglecting for the moment any change in $R$ along the orbit, the rotational-velocity gradient of the cold gas can be estimated as

$$\frac{\Delta v_\varphi}{\Delta z} = \frac{\Delta v}{\langle z_{\rm max} \rangle}\,, \tag{5}$$

where $\Delta v \equiv v(t_{\rm orb}) - v_0$ is the difference between the centroid velocity of the cold gas after $t_{\rm orb}$ and its initial velocity. In the hypothetical case of a static corona ($v_0 = 200\,{\rm km\,s^{-1}}$) $\Delta v \approx 40\,{\rm km\,s^{-1}}$ (see Fig. 4), so

$$\frac{\Delta v_\varphi}{\Delta z} \approx -20\,{\rm km\,s^{-1}\,kpc^{-1}}, \tag{6}$$

while in the case of a spinning corona (such that $v_0 = 75\,{\rm km\,s^{-1}}$)

$$\frac{\Delta v_\varphi}{\Delta z} \approx -7\,{\rm km\,s^{-1}\,kpc^{-1}}\,, \tag{7}$$

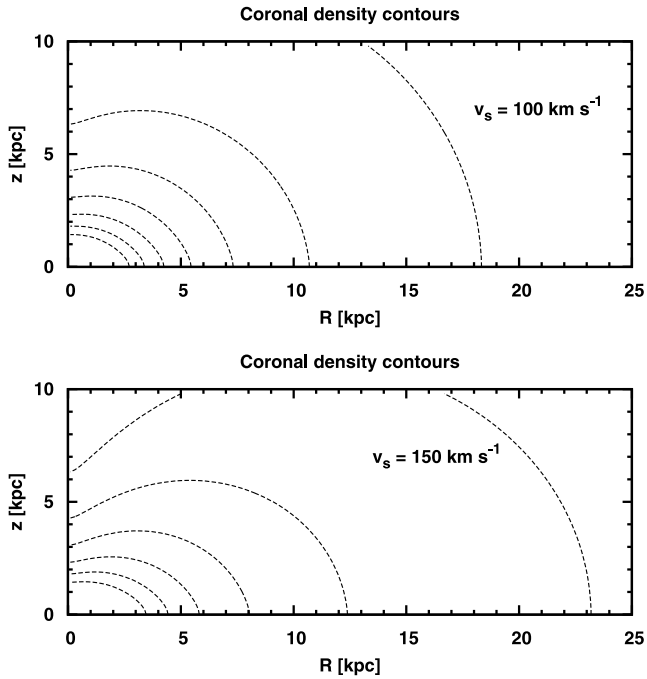


**Figure 6.** Meridional density contours of a rotating isothermal ($T = 2 \times 10^6$ K) corona in the Milky Way potential for two values of the asymptotic rotational velocity $v_{\rm s}$ (see equation 3). The density is normalized to the central ($R = z = 0$) value and the values on the contours are 0.45, 0.4, 0.35, 0.3, 0.25, 0.2, 0.15 (the lowest contour is not visible in the bottom panel).

based on the results of the dissipative simulation v75. We note that the effect of radiative cooling is crucial for the estimate of the gradient: using the adiabatic $v_0 = 75\,\mathrm{km\,s^{-1}}$ simulation we would get instead

$$\frac{\Delta v_\varphi}{\Delta z} \approx -3\,\mathrm{km\,s^{-1}\,kpc^{-1}}. \quad (8)$$

In the Milky Way the observed gradient is $\simeq -15\,\mathrm{km\,s^{-1}\,kpc^{-1}}$ (Marasco & Fraternali 2011), and similar values have been determined in external nearby galaxies. As mentioned, the above estimates neglect the variation of $R$ along the orbit, which by conservation of angular momentum induces a variation in $v_\varphi$. FB08 showed that this effect alone accounts for ∼50 per cent of the rotational gradient of the extraplanar gas. Thus, by adding this latter contribution to the estimate in equation (7), we get remarkably close the observed gradients.

On the basis of the above discussion we can conclude that: (i) larger velocity gradients are expected with increasing differences in rotational velocity between the clouds and the corona, (ii) as the relative velocity decreases, the drag becomes an inefficient process to decelerate the clouds, (iii) the radiative cooling of the gas has the effect of increasing the gradient to values which are very close to those required by the observations, and therefore (iv) the observed gradient can be explained only by a combination of cooling and drag. Overall, our results are consistent with the scenario developed in FB08, in which the accretion of gas by fountain clouds is the cause of the lagging kinematics of extraplanar gas in disc galaxies.

## 5 SUMMARY AND CONCLUSIONS

In this paper we studied the process of the momentum transfer between cold clouds ejected from the disc and the corona of disc galaxies like the Milky Way, which has a significant impact on the kinematics of both the coronal and the cold extraplanar gas. In particular, we presented two-dimensional hydrodynamical simulations of cloud–corona interaction. In the more realistic simulations the gas is allowed to cool radiatively, but, for comparison, we also considered the corresponding adiabatic cases. The simulations are similar, but significantly improved, with respect to those carried out by M10: here we explored a range of relative speeds between the cloud and the hot medium (50–200 $\mathrm{km\,s^{-1}}$), we followed the evolution of the system for longer time (60 Myr), we treated the metallicity as a dynamical variable (assigning initially to the cloud a metallicity ten times higher than that of the ambient gas) and we accounted for the variation with temperature of the fluid's molecular weight $\mu$.

From the simulations we draw the following conclusions.

(i) There is a relative velocity threshold of about 75 $\mathrm{km\,s^{-1}}$ between the cloud and the ambient medium, below which the corona stops absorbing momentum.

(ii) Radiative cooling is crucial for the existence of such velocity threshold: in adiabatic simulations the momentum transfer from the cloud to the hot gas is quite efficient at all explored relative speeds.

(iii) The actual value of the velocity threshold for Milky Way like galaxies depends on the coronal density: *less dense coronae have a lower velocity threshold*. In particular, in the interval of coronal densities explored by our simulations $v_{\mathrm{th}} \sim 50$–85 $\mathrm{km\,s^{-1}}$.

The process studied here has an important consequence on the kinematics of the corona. The corona cannot be static, otherwise the momentum transfer from the cold clouds would be very effective, but it cannot be rotating at a speed close to the rotation speed of the disc, because at low relative disc-corona (and thus cloud–corona) velocity the cooling hampers any momentum transfer. In a galaxy like the Milky Way we expect the corona to lag, in the inner regions, by ∼100 $\mathrm{km\,s^{-1}}$ with respect to the cold disc at $z \simeq 2$ kpc. Such a spinning corona must be characterized by a significantly flattened density distribution: based on simple isothermal models, we estimate values of the axis ratios of its isodensity surfaces in the range 0.5–0.7.

Due to interaction with the corona, fountain clouds gain mass and decelerate: based on our calculations, this effect can account for $\approx -7\,\mathrm{km\,s^{-1}\,kpc^{-1}}$ of the vertical gradient in rotational speed of the extraplanar gas in disc galaxies like the Milky Way. Such a value can be sufficient to reconcile purely ballistic fountain models with the observed kinematics of the H I extraplanar gas, giving further support to the 'fountain plus accretion' model of FB08.

In conclusion, we think that the presented results contribute quantitatively to refine an emerging consistent scenario in which galactic fountains, cold extraplanar gas and galactic coronae are strictly interlaced. This scenario makes specific predictions that can be tested in the future with soft X-ray observations detecting the elusive galactic coronae and with improved H I measures of the cold extraplanar gas. From the theoretical point of view, the next step will be the extension to three dimensions of the two-dimensional calculations here presented, and ideally one would like to realize 'global' simulations, in which the entire galaxy is modelled, with supernova-driven fountain clouds orbiting through the hot coronal medium under the effect of the galactic gravitational field.

## ACKNOWLEDGMENTS

We acknowledge the CINECA Award N.HP10CINIJ0, 2010 for the availability of high performance computing resources and support. FM, FF, CN and LC are supported by the MIUR grant PRIN 08.

## REFERENCES

Anderson M. E., Bregman J. N., 2010, ApJ, 714, 320
Barnabè M., Ciotti L., Fraternali F., Sancisi R., 2006, A&A, 446, 61
Binney J., Nipoti C., Fraternali F., 2009, MNRAS, 397, 1804
Binney J., Tremaine S., 2008, Galactic Dynamics, 2nd edn. Princeton Univ. Press, Princeton
Bregman J. N., 1980, ApJ, 236, 577
Bregman J. N., Lloyd-Davies E. J., 2007, ApJ, 669, 990
Collins J. A., Benjamin R. A., Rand R. J., 2002, ApJ, 578, 98
Del Zanna L., Bucciantini N., 2002, A&A, 390, 1177
Del Zanna L., Zanotti O., Bucciantini N., Londrillo P., 2007, A&A, 473, 11
Fox A. J., Savage B. D., Wakker B. P., 2006, ApJS, 165, 229
Fraternali F., 2009, in Andersen J., Bland-Hawthorn J., Nordström B. eds, Proc. IAU Symp. 254, New Evidence for Halo Gas Accretion on to Disc Galaxies. Astron. Soc. Pac. San Francisco p. 255
Fraternali F., Binney J. J., 2006, MNRAS, 366, 449
Fraternali F., Binney J. J., 2008, MNRAS, 386, 935 (FB08)
Fraternali F., Oosterloo T. A., Sancisi R., Swaters R., 2005, in Braun R., ed., ASP Conf. Ser. Vol. 331, The Extra-planar Neutral Gas in the Edge-on Spiral Galaxy NGC 891. Astron. Soc. Pac., San Francisco, p. 239
Fukugita M., Hogan C. J., Peebles P. J. E., 1998, ApJ, 503, 518
Fukugita M., Peebles P. J. E., 2004, ApJ, 616, 643
Heald G. H., Rand R. J., Benjamin R. A., Bershady M. A., 2007, ApJ, 663, 933
Houck J. C., Bregman J. N., 1990, ApJ, 352, 506
Kamphuis P., 2008, PhD thesis, Univ. Groningen
Kaufmann T., Mayer L., Wadsley J., Stadel J., Moore B., 2006, MNRAS, 370, 1612
Komatsu E., et al., 2009, ApJS, 180, 330

Lebovitz N. R., 1967, ARA&A, 5, 465
Marasco A., Fraternali F., 2011, A&A, 525, A134
Marinacci F., Binney J., Fraternali F., Nipoti C., Ciotti L., Londrillo P., 2010a, MNRAS, 404, 1464 (M10)
Marinacci F., Fraternali F., Ciotti L., Nipoti C., 2010b, MNRAS, 401, 2451
Melioli C., Brighenti F., D'Ercole A., de Gouveia Dal Pino E. M., 2009, MNRAS, 399, 1089
Nipoti C., 2010, MNRAS, 406, 247
Oosterloo T., Fraternali F., Sancisi R., 2007, AJ, 134, 1019
Rasmussen A., Kahn S. M., Paerels F., den Herder J., de Vries C., 2003, BAAS, 35, 605
Sarazin C. L., 2009, X-ray emission from Clusters of Galaxies. Cambridge Univ. Press, Cambridge
Sembach K. R., et al., 2003, ApJS, 146, 165
Shapiro P. R., Field G. B., 1976, ApJ, 205, 762
Shull J. M., Jones J. R., Danforth C. W., Collins J. A., 2009, ApJ, 699, 754
Spitzer L., Jr, 1956, ApJ, 124, 20
Struck C., Smith D. C., 2009, MNRAS, 398, 1069
Sutherland R. S., Dopita M. A., 1993, ApJS, 88, 253
Swaters R. A., Sancisi R., van der Hulst J. M., 1997, ApJ, 491, 140
Tassoul J.-L., 1978, Theory of Rotating Stars. Princeton Univ. Press, Princeton
Yao Y., Nowak M. A., Wang Q. D., Schulz N. S., Canizares C. R., 2008, ApJ, 672, L21

This paper has been typeset from a TEX/LATEX file prepared by the author.